Linear Analysis of Ordinary Bridges Crossing Fault-Rupture Zones

Rakesh K. Goel, F.ASCE[1]; and Anil K. Chopra, M.ASCE[2]

Abstract: Rooted in structural dynamics theory, two approximate procedures for estimating peak responses of linearly elastic "ordinary" bridges crossing fault-rupture zones are presented: response spectrum analysis (RSA) procedure and a linear static analysis procedure. These procedures estimate the peak response by superposing peak values of quasi-static and dynamic responses. The peak quasi-static response in both procedures is computed by static analysis of the bridge with peak values of all support displacements applied simultaneously. In RSA, the peak dynamic response is estimated by dynamic analysis including all significant modes, which is simplified in the latter procedure to static analysis of the bridge for appropriately selected forces; usually only one mode—the most dominant mode—is sufficient in the RSA procedure. Appearing in these procedures is the "effective" influence vector that differs from the influence vector for spatially uniform excitation, and the response spectrum used in the RSA procedure differs from the standard California Department of Transportation (CALTRANS) spectrum. Both of these simplified procedures provide estimates of peak response that are close enough to results of the "exact" response history analysis to be useful for practical application.

Introduction

Recent earthquakes have demonstrated the vulnerability of bridges that cross fault-rupture zones. Several bridges were seriously damaged as a result of rupture of causative faults in the 1999 Chi-Chi Earthquake (EERI 2001; Yen 2002), 1999 Kocaeli earthquake (EERI 2000), and the 1999 Duzce Earthquake (Ghasemi et al. 2000). Although avoiding building bridges across faults may be the best practice, it may not always be possible to do so, especially in regions of high seismicity, such as California. It is estimated that more than 5% of all bridges in California may either cross faults or lie in very close proximity to fault-rupture zones.

Bridges crossing fault-rupture zones will experience ground offset across the fault and hence spatially varying ground motion. Although site-specific seismological studies to define spatially varying ground motions and rigorous nonlinear response history analysis (RHA) are necessary for important bridges on "lifeline" routes, such investigations may be too onerous for "ordinary" bridges whose design is governed by the CALTRANS Seismic Design Criteria (SDC) (CALTRANS 2006). Ordinary bridges are defined as normal weight concrete bridges with span lengths less than 90 m supported on the substructure by pin/rigid connections or conventional bearings. The bent caps of ordinary bridges terminate inside of the exterior girders, and their foundations consist of spread footings, piles, or pile shafts with underlying soil that is not susceptible to liquefaction, lateral spreading, or scour. A large fraction of bridge inventory in California falls in the category of ordinary bridges. For such structures, simplified procedures for estimating seismic demands are needed to facilitate their seismic evaluation and design.

Gloyd et al. (2002) proposed a procedure that requires estimation of seismic demands for two additional load cases, without providing any structural-dynamics-based justification for the proposed load cases. Under the guidance of a technical advisory panel, this approach was used by the CALTRANS engineers and project consultants to design bridges in the SR210/I-215 interchange in San Bernardino, Calif.

The overall objective of this research investigation is to develop rational, simplified methods—simpler than the RHA—rooted in structural dynamics theory, for estimating seismic demand of bridges crossing fault-rupture zones. This paper presents such simplified analysis procedures for bridges, assuming they remain linearly elastic, which are extended in a companion paper to estimate seismic demands for bridges responding in their inelastic range (Goel and Chopra 2009). Utilizing special features of the spatially varying ground motions that are expected in fault-rupture zones, the procedures developed in this paper are shown to be accurate in estimating the peak response of eight linearly elastic bridges crossing fault-rupture zones.

Structural Systems and Modeling

The structural systems considered in this investigation were as follows: (1) a three-span symmetric bridge [Fig. 1(a)]; (2) a three-span unsymmetric bridge [Fig. 1(b)]; (3) a four-span symmetric bridge [Fig. 1(c)]; and a four-span unsymmetric bridge [Fig. 1(d)]. These bridges are supported on abutments at the two ends

[1]Professor, Dept. of Civil and Environmental Engineering, California Polytechnic State Univ., San Luis Obispo, CA 93407-0353. E-mail: rgoel@calpoly.edu

[2]Johnson Professor, Dept. of Civil and Environmental Engineering, Univ. of California, Berkeley, CA 94720. E-mail: chopra@ce.berkeley.edu

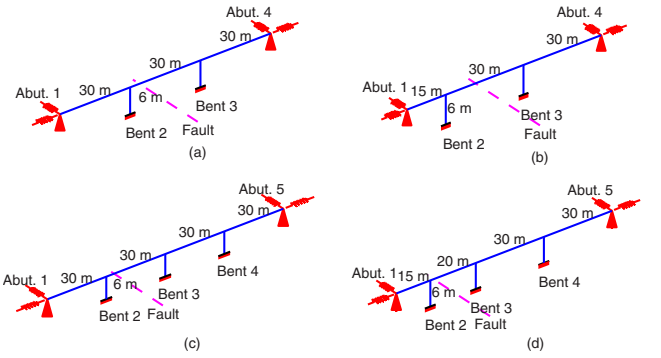

Fig. 1. Bridges considered: (a) three-span symmetric bridge, (b) three-span unsymmetric bridge; (c) four-span symmetric bridge; and (d) four-span unsymmetric bridge

and intermediate single-column bents. The span lengths and bent heights are shown in Fig. 1. The bases of columns in the bents were fixed [restraint for all 6 degrees-of-freedom (DOFs)]. The deck, which is expected to accommodate two traffic lanes, was selected as a 13 m wide and 1.2 m deep multicell box girder. The columns selected were 1.5 m diameter circular sections with helical transverse (or hoop) steel and longitudinal steel arranged at their periphery. The area of longitudinal steel was selected as 3% of the gross columns area and hoop steel was selected as 1% of the column volume to represent well-confined columns. The deck and column section properties, which are described in further details elsewhere (Goel and Chopra 2008a,b), are typical of many bridges in California. The fault was assumed to be located between Bents 2 and 3 of the selected bridges (Fig. 1). Note that the exact location of the fault between the two bents is not needed because, as demonstrated later in this paper, motions at various supports of the bridge are not affected by this location due to proportionality of motions on two sides of the fault.

The selected bridge systems were analyzed using the structural analysis software Open System for Earthquakes Engineering Simulation (OpenSees) (McKenna and Fenves 2001). The box girder and columns were modeled by linearly elastic beam column elements. In order to capture the distribution of mass along the length of the box girder, five elements per span were used. Consistent with CALTRANS recommendations (CALTRANS 2006), the gross values for moment of inertia and polar moment of inertia were used for the prestressed multicell box girder. The columns were modeled with single elements with the effective moment of inertia obtained from their section moment–curvature analysis. The restraint provided by the abutments was modeled with linear springs in the transverse and longitudinal directions, with spring stiffness computed according to the CALTRANS recommendations (CALTRANS 2006); details are available in recent publications by Goel and Chopra (2008a,b).

As shear keys significantly influence the seismic behavior of bridges, it is important that they be included in the structural model. A recent investigation (Goel and Chopra 2008b) examined seismic behavior of bridges in fault-rupture zones for three shear-key cases—without shear keys, with elastic shear keys, and with nonlinear shear keys. The first case assumed that the shear keys would break off upon initiation of design ground shaking and thus provide no transverse restraint. The second case assumed that the shear keys are strong enough to remain linear elastic and thus provide transverse restraint throughout the ground shaking. The third case assumed that the shear keys follow a nonlinear force–deformation behavior during design ground shaking. It was found

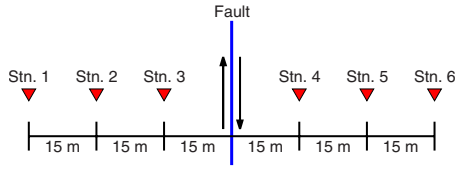

Fig. 2. Location of stations across the fault where spatially varying ground motions were simulated

that the seismic demands for a bridge with nonlinear shear keys can generally be bounded by the demands computed for two shear-key cases: elastic shear keys and without shear keys.

Because of the difficulty in accurately modeling highly nonlinear and brittle behavior of shear keys, the two extreme cases (without shear keys and with elastic shear keys) that permit linear elastic modeling of a bridge and bound the response of a bridge with nonlinear shear keys are considered here. Details on shear key behavior and computer modeling are available in Goel and Chopra (2008b).

The four selected bridges (three-span symmetric, three-span unsymmetric, four-span symmetric, and four-span unsymmetric) and the aforementioned two shear-key cases provide a total of eight bridge configurations: (1) three-span symmetric bridge without shear keys; (2) three-span symmetric bridge with elastic shear keys; (3) three-span unsymmetric bridge without shear keys; (4) three-span unsymmetric bridge with elastic shear keys; (5) four-span symmetric bridge without shear keys; (6) four-span symmetric bridge with elastic shear keys; (7) four-span unsymmetric bridge without shear keys; and (8) four-span unsymmetric bridge with elastic shear keys. Seismic responses of these eight bridges, referred to as Bridges 1–8, are examined later in this paper. These bridges facilitate evaluation of the presented procedures for varying parametric conditions: number of spans (three-span versus four-span bridges); asymmetry in bridge geometry (symmetric versus asymmetric bridges); and shear-key condition (elastic shear keys versus no shear keys).

Response Quantities

The response quantities considered in this investigation are the column drift and deck displacement at the abutment. The column drift, which indicates deformation demand in the column, is defined as the displacement at top of the column relative to its base displacement. The deck displacement at the abutment, which is used to estimate the relative displacement of the deck from the abutment, is defined as the displacement of the deck at the abutment relative to the displacement at the top of the abutment.

Ground Motions

Ground motions are to be defined at bridge supports in close proximity to the fault (Fig. 1). Unfortunately, to date, ground motions have never been recorded at such fine spacing in close proximity to the causative fault. For this investigation, motions were simulated at stations spaced 15 m apart (Fig. 2) due to a magnitude 6.5 earthquake in the fault-normal, fault-parallel, and vertical directions across a fault-rupture zone (Dreger et al. 2007). Resulting from this simulation, the fault-parallel and fault-normal components of ground acceleration, velocity, and displacement at Stations 1–6 are discussed next. The vertical motions are not

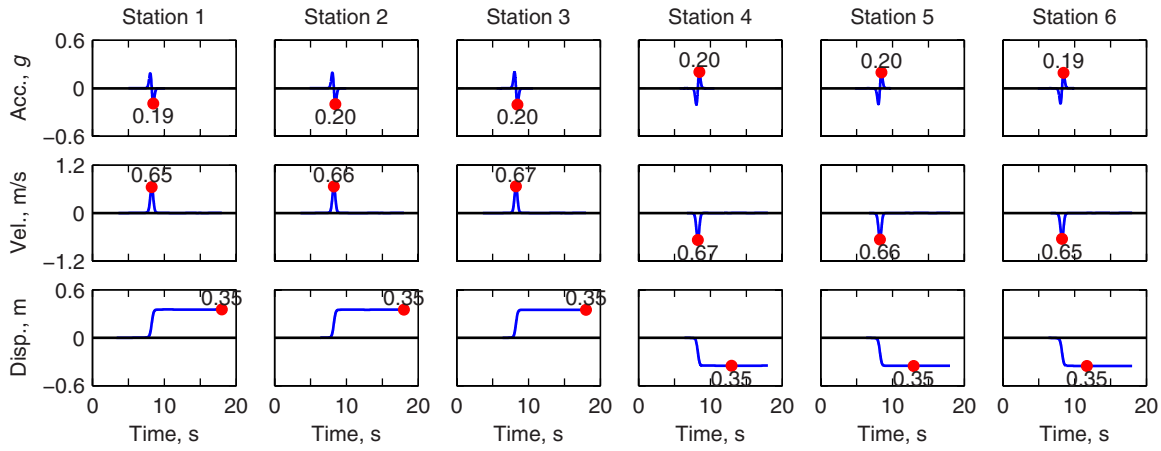

Fig. 3. Displacement, velocity, and acceleration in fault-parallel direction at six stations across a strike-slip fault during magnitude 6.5 earthquake

considered in this investigation because they do not lead to column drift or deck displacement at abutment, the two response quantities of interest.

Motions across Vertical Strike-Slip Faults

The fault-parallel motions across a strike-slip fault exhibit time variation of ground displacement that is a gradual step function, ground velocity that is a single-sided pulse, and ground acceleration that is a double-sided pulse (Fig. 3). As expected, the ground motion in fault-rupture zones exhibits a permanent displacement (or static offset) that occurs over rise-time T_r. At a distance close to the fault, the static displacement is one-half of the average slip of the fault. Both the static-offset (or average slip) and rise-time are related to the earthquake magnitude (Somerville et al. 1999; Goel and Chopra 2008a).

Fig. 3 also shows that the simulated fault-parallel motions are antisymmetric about the fault plane, i.e., fault-parallel motions at stations located equidistant from the fault, but on opposite sides are essentially the same time functions, but are opposite in algebraic signs. Further, the motions at Stations 1–3 on one side of the fault are essentially identical, and motions at Stations 4–6 on the other side of the fault are also almost identical. This indicates that motions at various stations (or locations) across the fault are essentially proportional to each other. Thus, the displacement at support l

$$u_{gl}(t) = \alpha_l u_g(t) \tag{1}$$

in which $u_g(t)$=displacement history of motion at a reference location and α_l=proportionality constant for the lth support. The support motion defined by Eq. (1) is referred to as proportional multiple-support excitation in rest of this paper. The validity of this hypothesis is demonstrated in Fig. 4, where motions obtained from Eq. (1), with Station 6 selected as the reference location, are compared with the simulated motions. The numerical values of α_l, computed as the ratio of the peak displacements at the lth station and at the reference location (Station 6) noted in Fig. 4 are close to +1 or −1.

The fault-normal displacements across a strike-slip fault are essentially identical across the fault (Fig. 5). Therefore, such motions may be treated as a spatially uniform excitation. The fault-normal displacements across a vertical strike-slip fault generally do not exhibit static-offset, except at locations close to the start and end of the fault rupture; such motions are not included here for brevity, but are available in another report (Dreger et al. 2007).

Motions across Other Types of Faults

The validity of Eq. (1) has been found to be approximately valid for fault-parallel component of ground displacements across other types of faults (Goel and Chopra 2008a), i.e., faults with other dip and rake angles. Note that dip=90°, rake=180° for a strike-slip fault; dip angle is the angle of the fault plane with respect to a horizontal plane on the surface of the earth, and rake angle is the angle of slip direction on the fault with respect to a horizontal line on the fault surface. For faults other than strike-slip, however, α_l differs significantly from ±1. The fault-normal component of ground displacements across dipping faults also were found to exhibit similar trends: (1) displacements exhibit static offset and vary across the fault and (2) the spatially varying excitation can be modeled approximately as proportional multiple-support excitation with α_l differing from ±1. The motions on other types of faults considered in this investigation are those on a fault with dip=40°, rake=110°; description of these motions is available in Goel and Chopra (2008a).

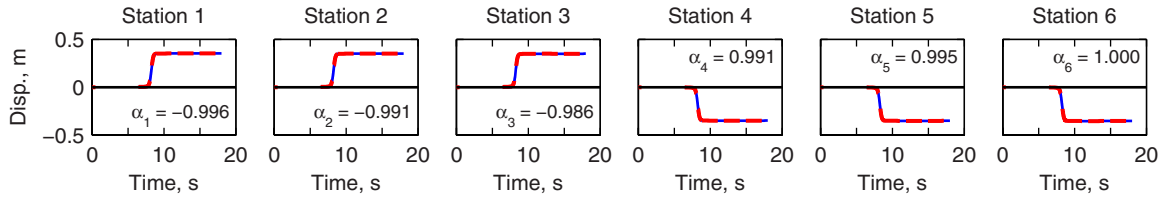

Fig. 4. Comparison of Eq. (1) (dashed line) with simulated displacements (solid line) in the fault parallel direction as a result of rupture on a strike-slip fault; α_l are as noted

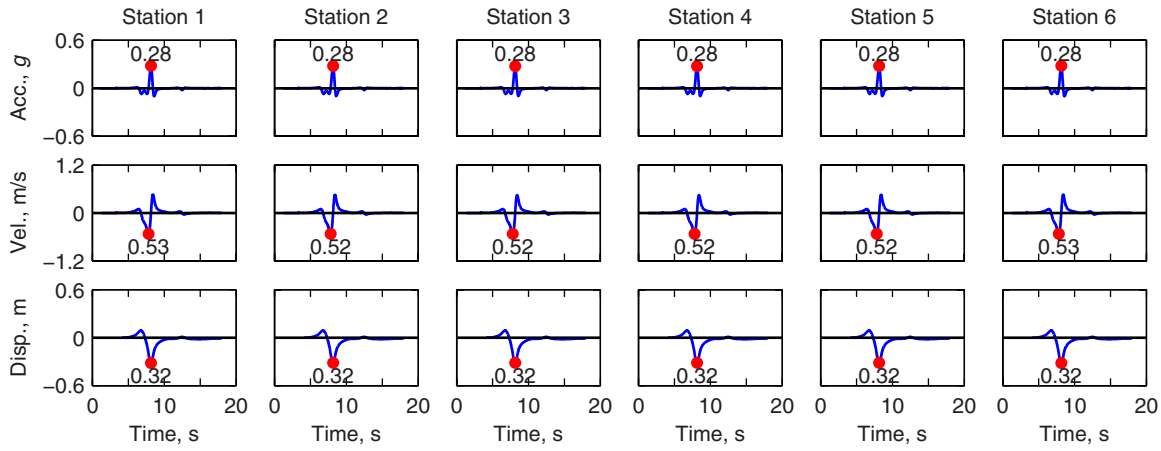

Fig. 5. Displacement, velocity, and acceleration in fault-normal direction at six stations across a strike-slip fault during magnitude 6.5 earthquake

Response Spectrum

Fig. 6 shows the pseudoacceleration response spectrum for the fault-parallel and fault-normal components of ground motion, with permanent offset, in very close proximity (say, roughly, 15 m) to the causative fault. The pseudoacceleration scale has been normalized by the peak ground acceleration ($A/\ddot{u}_{g0}$), and the period scale by the rise time (T_n/T_r). When presented in such normalized form, the spectrum is valid for earthquakes over a wide range of magnitudes (Goel and Chopra 2008a).

The CALTRANS SDC spectrum is inappropriate for the analysis of bridges crossing fault-rupture zones because it differs considerably from the response spectrum for expected ground motions. This becomes apparent by comparing the normalized response spectrum for ground motions in fault-rupture zones with the CALTRANS SDC spectrum (Fig. 7). It is useful to note that even bridges located in fault-rupture zones must be analyzed for near- or far-field motions resulting from faults that do not rupture all the way to the ground surface. For such analyses, the CALTRANS SDC spectrum may be appropriate. However, the CALTRANS SDC spectrum is not appropriate for analysis of the bridge for motions resulting from rupture of a fault between its supports.

Note that the various spectra in Fig. 7 are normalized by dividing the spectral acceleration, A, with the peak ground acceleration, $\ddot{u}_{g0}$. Further, the CALTRANS SDC spectrum included in Fig. 7 is for peak ground acceleration (PGA) of $0.4g$, soil type B, and earthquake magnitude 6.5 ± 0.25. Although CALTRANS SDC provides spectrum for PGA values in the range of $0.1-0.6g$ for each earthquake magnitude and soil type, only one spectrum for $0.4g$ PGA is included here for clarity.

Response History Analysis

Multiple-Support Excitation (Chopra 2007, Sec 9.7)

Equations governing the motions of a linearly elastic structure subjected to multiple-support excitation are formulated by separating the displacements at the N DOFs of the superstructure in two parts: (1) $\mathbf{u}^s$ the quasi-static displacements due to static application of the displacements $\mathbf{u}_g$ imposed at the supports; and (2) $\mathbf{u}$ the dynamic displacements, governed by

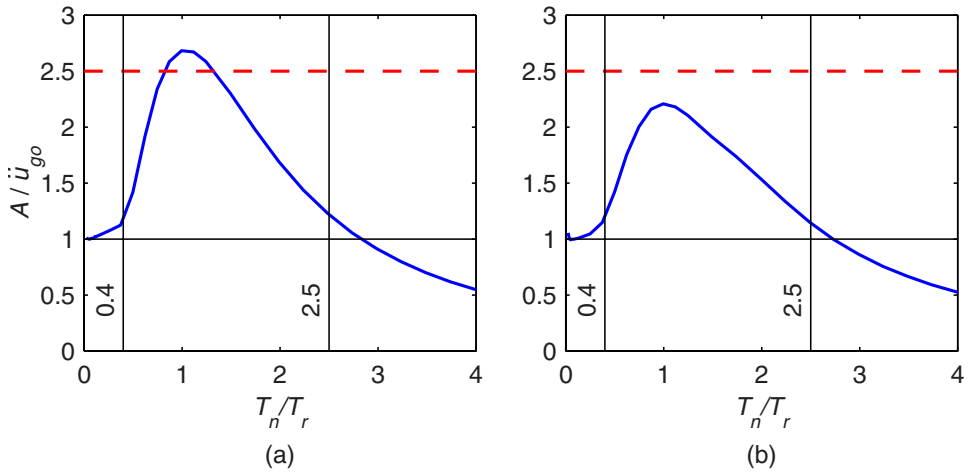

Fig. 6. Normalized 5%-damped elastic response spectrum for ground motions in fault-rupture zones: (a) fault-parallel component on a vertical strike-slip fault with dip of 90° and rake of 180°; (b) fault-normal component on a fault with dip of 40° and rake of 110°

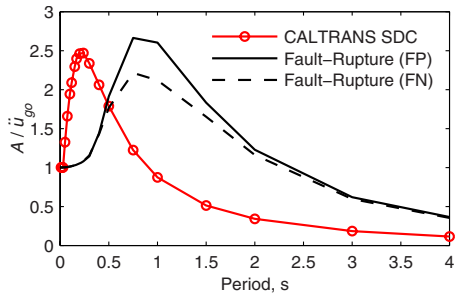

Fig. 7. Comparison of normalized 5%-damped elastic response spectrum for ground motions in fault-rupture zone with the CALTRANS SDC spectrum

$$\mathbf{m}\ddot{\mathbf{u}} + \mathbf{c}\dot{\mathbf{u}} + \mathbf{k}\mathbf{u} = -\mathbf{m}\sum_{l=1}^{N_g} \boldsymbol{\iota}_l \ddot{u}_{gl}(t) \tag{2}$$

where $\mathbf{m}$, $\mathbf{c}$, and $\mathbf{k}$ = mass, damping, and stiffness matrices corresponding to structural DOF; $\ddot{u}_{gl}(t)$ = acceleration at support l; $\boldsymbol{\iota}_l$ = influence vector defined as the displacements in the superstructure DOF due to unit displacement at the lth support DOF; and N_g = number of components of support displacements. The total response is then given by

$$\mathbf{u}^t(t) = \mathbf{u}^s(t) + \mathbf{u}(t) = \sum_{l=1}^{N_g} \boldsymbol{\iota}_l u_{gl}(t) + \sum_{l=1}^{N_g} \left[\sum_{n=1}^{N} \Gamma_{nl} \boldsymbol{\phi}_n D_{nl}(t) \right] \tag{3}$$

in which $D_{nl}(t)$ = deformation response of the nth-mode SDF system subjected to ground motion $\ddot{u}_{gl}(t)$; $\boldsymbol{\phi}_n$ = nth natural mode of vibration, and $\Gamma_{nl} = \boldsymbol{\phi}_n^T \mathbf{m}\boldsymbol{\iota}_l / \boldsymbol{\phi}_n^T \mathbf{m}\boldsymbol{\phi}_n$.

Proportional Multiple-Support Excitation

For excitation defined by Eq. (1), Eq. (2) simplifies to

$$\mathbf{m}\ddot{\mathbf{u}} + \mathbf{c}\dot{\mathbf{u}} + \mathbf{k}\mathbf{u} = -\mathbf{m}\boldsymbol{\iota}_{\text{eff}} \ddot{u}_g(t) \tag{4}$$

where the "effective" influence vector

$$\boldsymbol{\iota}_{\text{eff}} = \sum_{l=1}^{N_g} \alpha_l \boldsymbol{\iota}_l \tag{5}$$

is the vector of displacements at all structural degrees of freedom due to simultaneous static application of all support displacements with value equal to α_l at the lth support and $\ddot{u}_g(t)$ = acceleration at the reference support.

The right-hand side of Eq. (4) can be interpreted as effective earthquake forces

$$\mathbf{p}_{\text{eff}}(t) = -\mathbf{m}\boldsymbol{\iota}_{\text{eff}} \ddot{u}_g(t) \tag{6}$$

The spatial distribution of these effective forces is defined by the vector $\mathbf{s} = \mathbf{m}\boldsymbol{\iota}_{\text{eff}}$ and their time variation by $\ddot{u}_g(t)$. The force distribution $\mathbf{s}$ can be expanded as a summation of modal inertia force distribution $\mathbf{s}_n$ (Chopra 2007: Sec. 13.2)

$$\mathbf{m}\boldsymbol{\iota}_{\text{eff}} = \sum_{n=1}^{N} \mathbf{s}_n = \sum_{n=1}^{N} \Gamma_n \mathbf{m}\boldsymbol{\phi}_n \tag{7}$$

where $\Gamma_n = \boldsymbol{\phi}_n^T \mathbf{m}\boldsymbol{\iota}_{\text{eff}} / \boldsymbol{\phi}_n^T \mathbf{m}\boldsymbol{\phi}_n$. The effective earthquake forces can then be expressed as

$$\mathbf{p}_{\text{eff}}(t) = \sum_{n=1}^{N} \mathbf{p}_{\text{eff},n}(t) = \sum_{n=1}^{N} -\mathbf{s}_n \ddot{u}_g(t) \tag{8}$$

The contributions of the nth mode to $\mathbf{s}$ and to $\mathbf{p}_{\text{eff}}$ are

$$\mathbf{s}_n = \Gamma_n \mathbf{m}\boldsymbol{\phi}_n, \quad \mathbf{p}_{\text{eff},n}(t) = -\mathbf{s}_n \ddot{u}_g(t) \tag{9}$$

The response of a linearly elastic multi-degree-of-freedom system to $\mathbf{p}_{\text{eff},n}(t)$ is entirely in the nth mode, with no contributions from other modes. Thus

$$\mathbf{u}_n(t) = \Gamma_n \boldsymbol{\phi}_n D_n(t) \tag{10}$$

where $D_n(t)$ = deformation response of the nth-mode SDF system subjected to the reference ground motion $\ddot{u}_g(t)$. It is governed by

$$\ddot{D}_n + 2\zeta_n \omega_n \dot{D}_n + \omega_n^2 D_n = -\ddot{u}_g(t) \tag{11}$$

Any response quantity $r(t)$—deformations, internal element forces, etc.—can be expressed as

$$r_n(t) = r_n^{\text{st}} A_n(t) \tag{12}$$

where r_n^{st} denotes the modal static response, the static value of r due to external forces $\mathbf{s}_n$, and

$$A_n(t) = \omega_n^2 D_n(t) \tag{13}$$

is the pseudoacceleration response of the nth-mode SDF system (Chopra 2007; Sec. 13.1). The response of the system to the total excitation $\mathbf{p}_{\text{eff}}(t)$ is obtained by superimposing the modal responses given by Eqs. (10) and (12)

$$\mathbf{u}(t) = \sum_{n=1}^{N} \mathbf{u}_n(t) = \sum_{n=1}^{N} \Gamma_n \boldsymbol{\phi}_n D_n(t) \tag{14a}$$

$$r(t) = \sum_{n=1}^{N} r_n(t) = \sum_{n=1}^{N} r_n^{\text{st}} A_n(t) \tag{14b}$$

The total displacements of the structure are then given by

$$\mathbf{u}^t(t) = \mathbf{u}^s(t) + \mathbf{u}(t) = \boldsymbol{\iota}_{\text{eff}} u_g(t) + \sum_{n=1}^{N} \Gamma_n \boldsymbol{\phi}_n D_n(t) \tag{15}$$

Note that the responses to individual support motions appear in the summation over N_g in Eq. (2) but they are represented indirectly in the effective influence vector that affects Γ_n and $D_n(t)$ in Eq. (15).

Eq. (15) for total response of a bridge crossing fault-rupture zone to proportional multiple-support excitation resembles the following equation for a bridge located on one side of the fault subjected to spatially uniform excitation (Chopra 2007, Sec. 9.4):

$$\mathbf{u}^t(t) = \mathbf{u}^s(t) + \mathbf{u}(t) = \boldsymbol{\iota} u_g(t) + \sum_{n=1}^{N} \Gamma_n \boldsymbol{\phi}_n D_n(t) \tag{16}$$

where $\boldsymbol{\iota}$ = influence vector of displacements resulting from static application of a unit ground displacement simultaneously at all supports, and $\Gamma_n = \boldsymbol{\phi}_n^T \mathbf{m}\boldsymbol{\iota} / \boldsymbol{\phi}_n^T \mathbf{m}\boldsymbol{\phi}_n$. However, the influence vectors that appear explicitly in Eqs. (15) and (16) and implicitly in Γ_n and $D_n(t)$, are very different. In Eq. (15), $\boldsymbol{\iota}_{\text{eff}}$ represents the structural displacements due to static application of all support displacement with value equal to α_l at the lth support, which is antisymmetric about a strike-slip fault. In Eq. (16), $\boldsymbol{\iota}$ represents the structural displacements due to rigid body displacement of the base (or all support displacements) equal to 1, which is symmetric about the fault.

The accuracy of proportional multiple-support excitation approximation was evaluated by comparing bridge response computed by two methods of response history analysis: the "exact" Eq. (3) for multiple-support excitation and Eq. (15), which is based on approximating the excitation by Eq. (1). Although results are not included here for brevity, it showed that the proportional multiple-support excitation provides accurate results (Goel and Chopra 2008a).

Estimation of Peak Response

Of primary interest in practical design of new bridges or evaluation of existing bridges crossing fault-rupture zones is their peak response to earthquake excitation. A procedure specially designed for bridges crossing fault-rupture zones is proposed where the peak value of the total response, $\mathbf{u}_o^t$ and r_o^t, is estimated by adding peak values of the quasi-static response, $\mathbf{u}_o^s$ and r_o^s, and dynamic response, $\mathbf{u}_o$ and $\mathbf{r}_o$

$$\mathbf{u}_o^t \simeq \mathbf{u}_o^s + \mathbf{u}_o, \quad r_o^t \simeq r_o^s + r_o \tag{17}$$

Such superposition of peak quasi-static and dynamic responses is reasonable because for motions in fault-rupture zones, the peak value of the dynamic part of the response generally occurs during the time phase after the quasi-static part of the response reaches, and maintains, its peak value (Goel and Chopra 2008a). Eq. (17) may be interpreted as a special case of the multisupport response spectrum analysis procedure (Der Kiureghian and Neuenhofer, 1992) for ground motions in fault-rupture zones because the support motions and peak values of quasi-static and dynamic responses are correlated (A. Neuenhofer, personal communication, 2007).

The peak value of the quasi-static response, r_o^s, is due to static application of the peak values of ground displacements, $\alpha_l u_{go}$, simultaneously at all supports where u_{go}=peak value of the ground displacement at the reference support. Presented next are two procedures to determine the peak value of dynamic response: response spectrum analysis and static analysis.

Response Spectrum Analysis (RSA) Procedure

The peak dynamic response is estimated by using the square-root-of-sum-of-square (SRSS) or complete-quadratic-combination (CQC) rule, as appropriate, to combine the peak modal responses. Although not rigorously valid for ground motions in close proximity to the causative fault, these modal combinations will be used and their accuracy evaluated. The peak value of the dynamic response, r_o, is computed by implementing the following steps:

1. Compute the vibration periods, T_n, and mode shapes, $\boldsymbol{\phi}_n$, of the bridge.
2. Identify the significant modes that need to be considered in the dynamic analysis based on the modal contribution factors as follows:
   - 2.1. Compute the effective influence vector, $\boldsymbol{\iota}_{\text{eff}}$, the vector of displacements in the structural DOF obtained by static analysis of the bridge due to support displacements α_l, applied simultaneously in the appropriate direction: fault-parallel or fault-normal;
   - 2.2. Compute the static response, r^{st}, by static analysis of the bridge due to forces $\mathbf{m}\boldsymbol{\iota}_{\text{eff}}$ applied at the structural DOF;
   - 2.3. Compute the modal static response, r_n^{st}, from static analysis of the bridge due to forces $\mathbf{s}_n = \Gamma_n \mathbf{m}\boldsymbol{\phi}_n$ applied at the structural DOF, where $\Gamma_n = \boldsymbol{\phi}_n^{\text{T}}\mathbf{m}\boldsymbol{\iota}_{\text{eff}} / \boldsymbol{\phi}_n^{\text{T}}\mathbf{m}\boldsymbol{\phi}_n$;
   - 2.4. Compute the modal contribution factor for the nth mode, $\bar{r}_n = r_n^{\text{st}} / r^{\text{st}}$ (Chopra 2007: Sec. 12:10);
   - 2.5. Repeat Steps 2.3 and 2.4 for all modes; and
   - 2.6. Select the number of significant modes, J, such that the error in the static value response quantity r, $e_J = 1 - \sum_{n=1}^{J} \bar{r}_n$, is less than acceptable value, e.g., 0.05.
3. Compute the peak value of the nth mode dynamic response, $r_{no} = r_n^{\text{st}} A_n$ in which r_n^{st}=modal static response (Step 2.3) and A_n=ordinate of the pseudoacceleration spectrum for the reference support acceleration $\ddot{u}_g(t)$ corresponding to the nth-mode SDF system.
4. Repeat Step 3 for all significant modes identified in Step 2.
5. Combine the peak modal response by SRSS or CQC modal combination rule, as appropriate, to obtain the peak dynamic response, r_o.

Linear Static Analysis Procedure

To develop a procedure that is especially convenient for practical application, the RSA procedure is simplified by recognizing that: (1) In many cases, the individual modal responses in the RSA tend to attain their peak values at essentially the same time (Goel and Chopra 2008a) indicating that the algebraic sum of the peak responses (instead of CQC or SRSS combinations) should provide a reasonable estimate of the peak value of the combined response and (2) for most bridges, the value of A may be conservatively approximated by $A = 2.5\ddot{u}_{go}$ (Fig. 6). For such a case, the peak dynamic response can simply be computed by static analysis of the structure due to lateral forces $(\mathbf{p}_{\text{eff}})_o = 2.5\ \mathbf{m}\boldsymbol{\iota}_{\text{eff}}\ddot{u}_{go}$, which avoids computation of the vibration periods of the bridge.

Thus, the peak value of the dynamic response, r_o, is computed by implementing the following steps:

1. Compute the effective influence vector, $\boldsymbol{\iota}_{\text{eff}}$, as the vector of displacements in the structural DOF obtained by static analysis of the bridge due to support displacements α_l, applied simultaneously.
2. Estimate the dynamic response r_o by static analysis of the bridge due to lateral forces=$2.5\ \mathbf{m}\boldsymbol{\iota}_{\text{eff}}\ddot{u}_{go}$.

Significant Vibration Modes

Presented in this section are vibration properties—periods, mode shapes, effective modal masses, and modal contribution factor values—of the selected bridges. These vibration properties are used to identify the modes that contribute significantly to the total response.

Mode Shapes, Vibration Periods, and Effective Modal Masses

The first six vibration periods and modes of the selected bridges, each with two shear key conditions, are presented in Figs. 8 and 9. Also included for each mode are the effective modal mass (as a fraction of the total mass) in the longitudinal, transverse, and vertical directions. The bridge modes may be categorized by their primary motion—transverse, longitudinal, torsional, or vertical—or coupled motion such as longitudinal-vertical or transverse-torsional. Category of a mode shape may be identified from deflected shape of the bridge and effective modal masses. For example, a transverse, longitudinal, and vertical mode shape exhibits deflection and nonzero value of the effective modal mass in the transverse [see Mode 1 in Fig. 8(a)], longitudinal [see

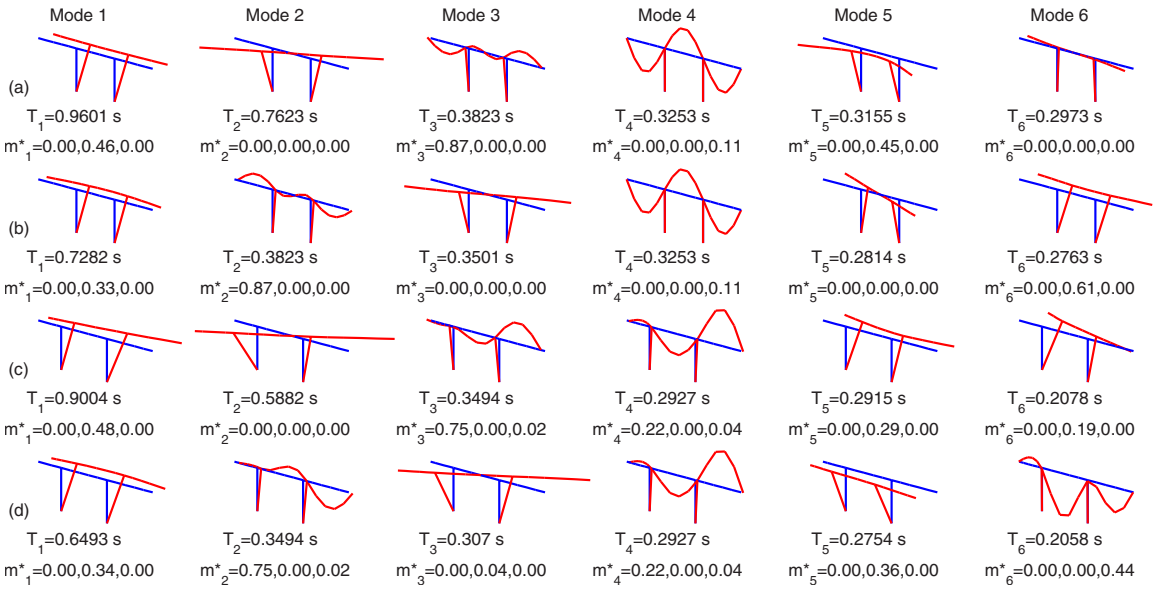

Fig. 8. Mode shapes, vibration periods, and effective modal masses (in longitudinal, transverse, and vertical direction) as a fraction of the total mass of three-span bridges: (a) symmetric without shear keys; (b) symmetric with elastic shear keys; (c) unsymmetric without shear keys; and (d) unsymmetric with elastic shear keys

Mode 3 in Fig. 8(a)], and vertical [see Mode 4 in Fig. 8(a)] direction, respectively; a purely torsional mode exhibits rotation about the vertical axis and zero values of the effective modal mass in all three directions [see Mode 2 in Fig. 8(a)]; a coupled longitudinal-vertical mode exhibits motions and nonzero values of the effective modal mass in the longitudinal and vertical direction [see Mode 4 in Fig. 8(c)]; and a coupled transverse-torsional mode exhibits rotational and transverse motions but nonzero value of the effective modal mass in the transverse direction [see Mode 1 in Fig. 8(c)].

Although the fundamental mode of symmetric bridges exhibits no coupling with torsional motion [Mode 1 in Figs. 8(a and b, 9(a, and b)], coupling occurs between transverse and torsional motions for unsymmetric bridges [Figs. 8(c and d, 9(c, and d)]. Further, both symmetric and unsymmetric bridge exhibit a predominantly torsional mode with no or little coupling with transverse motion [Mode 2 in Figs. 8(a–d) and 9(a and c), and Mode 3 in Figs. 9(b and d)]. Some transverse modes exhibit flexural deformation of

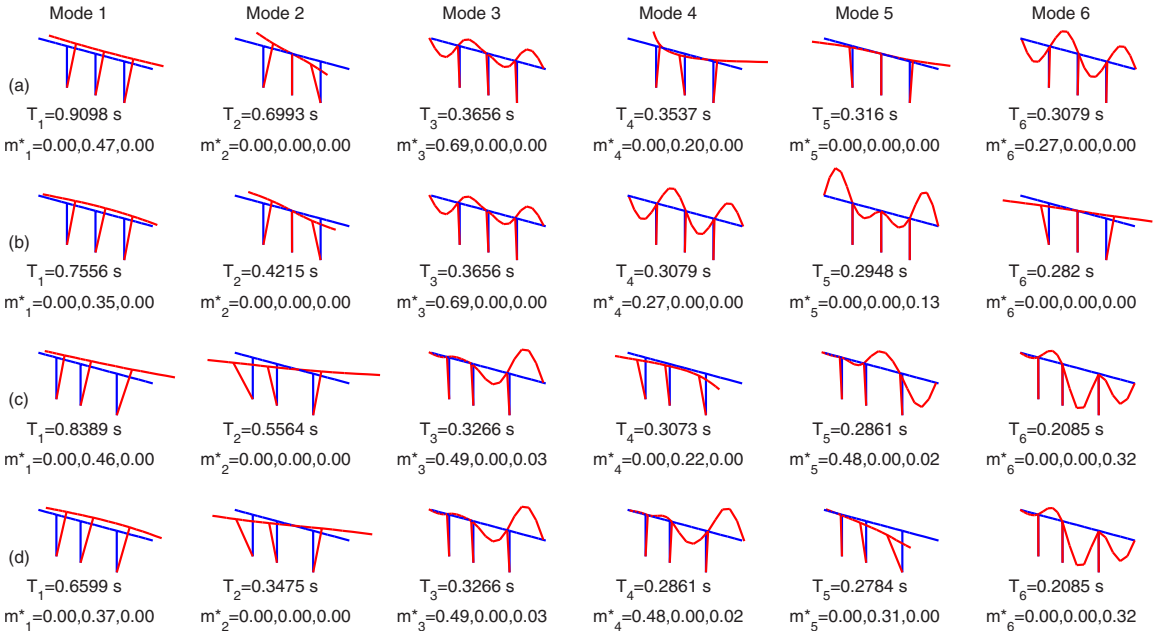

Fig. 9. Mode shapes, vibration periods, and effective modal masses (in longitudinal, transverse, and vertical direction) as a fraction of the total mass of four-span bridges: (a) symmetric without shear keys; (b) symmetric with elastic shear keys; (c) unsymmetric without shear keys; and (d) unsymmetric with elastic shear keys

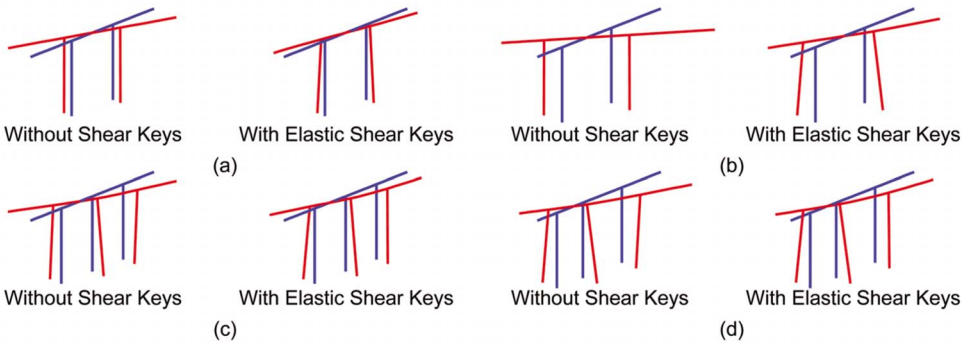

Fig. 10. Deflected shapes of bridges crossing fault-rupture zones associated with the effective influence vector for excitation in fault-parallel direction: (a) three-span symmetric; (b) three-span unsymmetric; (c) four-span symmetric; and (d) four-span unsymmetric

the deck [e.g., Mode 5 in Figs. 8(a) and 9(a)] with the effect being prominent for bridges with elastic shear keys [Mode 1 in Figs. 8(b and d) and 9(b and d)].

Modal Contribution Factors and Significant Modes

Associated with the effective influence vector for fault-parallel motions, the deflected shapes of the selected bridges, each with two shear key cases, are presented in Figs. 10 and 11 for proportional multiple-support excitation for bridges crossing fault--rupture zones and spatially uniform excitation for bridges on one side of the fault, respectively. The effective influence vectors exhibit significant torsional motion about the vertical axis for a bridge across a fault (Fig. 10), in contrast to the translational motion of the bridge on one side of the fault (Fig. 11).

Tables 1–4 list the values of the modal contribution factors for two selected responses (drift in Bent 2 and displacement at Abutment 1) for bridges crossing fault-rupture zones as well as bridges on one side of the fault, and fault-parallel ground motion; modes

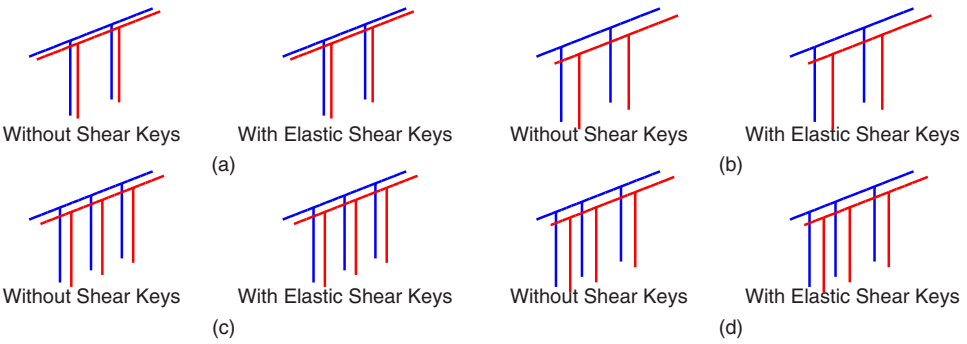

Fig. 11. Deflected shapes of bridges on one side of the fault associated with the effective influence vector for excitation in fault-parallel direction: (a) three-span symmetric; (b) three-span unsymmetric; (c) four-span symmetric; and (d) four-span unsymmetric

Table 1. Modal Contribution Factors for Three-Span Symmetric Bridge and Strike-Slip Fault

	Bridge without shear keys					Bridge with shear keys				
		Across fault		One side			Across fault		One side	
Mode	Period (s)	Bent 2 drift	Abut 1 disp.	Bent 2 drift	Abut 1 disp.	Period (s)	Bent 2 drift	Abut 1 disp.	Bent 2 drift	Abut 1 disp.
1	0.960	0	0	*0.918*	*0.863*	0.728	0	0	*0.811*	*0.689*
2	0.762	*0.994*	*0.992*	0	0	0.382	0	0	0	0
3	0.382	0	0	0	0	0.350	*0.637*	*0.602*	0	0
4	0.325	0	0	0	0	0.325	0	0	0	0
5	0.315	0	0	*0.069*	0.155	0.281	*0.361*	*0.396*	0	0
6	0.297	0.005	0.008	0	0	0.276	0	0	*0.186*	*0.301*
7	0.268	0	0	0	0	0.268	0	0	0	0
8	0.196	0	0	0	0	0.196	0	0	0	0
9	0.184	0	0	0.005	−0.010	0.170	0	0	−0.004	0.030
10	0.158	0	0	0.007	−0.008	0.152	0	0	0.007	−0.020

Note: Results are presented for bridge with fault crossing between Bent 2 and Bent 3, and bridge on one side of fault.

Table 2. Modal Contribution Factors for Three-Span Unsymmetric Bridge and Strike-Slip Fault

	Bridge without shear keys					Bridge with shear keys				
		Across fault		One side			Across Fault		One side	
Mode	Period (s)	Bent 2 drift	Abut 1 disp.	Bent 2 drift	Abut 1 disp.	Period (s)	Bent 2 drift	Abut 1 disp.	Bent 2 drift	Abut 1 disp.
1	0.900	*−1.639*	*−0.397*	*0.890*	*0.837*	0.649	*0.098*	0.046	*0.833*	*0.843*
2	0.588	*2.647*	*1.394*	−0.027	*−0.055*	0.349	0	0	0	0
3	0.349	0	0	0	0	0.307	*0.879*	*0.869*	*−0.075*	*−0.160*
4	0.293	0	0	0	0	0.293	0	0	0	0
5	0.291	*−0.063*	−0.026	*0.091*	*0.146*	0.275	*−0.234*	*−0.117*	*0.138*	*0.149*
6	0.208	*0.053*	0.024	0.046	*0.081*	0.206	0	0	0	0
7	0.206	0	0	0	0	0.199	*0.252*	*0.180*	*0.103*	*0.159*
8	0.142	0	−0.002	0	0.001	0.140	−0.002	−0.008	0	0.003
9	0.128	0.001	0.007	0	−0.009	0.119	0.006	0.028	0.001	0.007
10	0.096	0	0	0	0	0.096	0	0.002	0	−0.001

Note: Results are presented for bridge with fault crossing between Bent 2 and Bent 3, and bridge on one side of fault.

Table 3. Modal Contribution Factors for Four-Span Symmetric Bridge and Strike-Slip Fault

	Bridge without shear keys					Bridge with shear keys				
		Across fault		One side			Across fault		One side	
Mode	Period (s)	Bent 2 drift	Abut 1 disp.	Bent 2 drift	Abut 1 disp.	Period (s)	Bent 2 drift	Abut 1 disp.	Bent 2 drift	Abut 1 disp.
1	0.910	*−0.401*	*−0.167*	*0.914*	*0.841*	0.756	*39.30*	*−0.363*	*0.839*	*0.655*
2	0.699	*1.384*	*1.102*	0	0	0.422	*−25.73*	*0.796*	0	0
3	0.366	0	0	0	0	0.366	0	0	0	0
4	0.354	0	0	0.038	*0.202*	0.308	0	0	0	0
5	0.316	0.042	*0.056*	0	0	0.295	0	0	0	0
6	0.308	0	0	0	0	0.282	*−17.64*	*0.661*	0	0
7	0.295	0	0	0	0	0.274	*3.860*	*−0.093*	*0.145*	*0.294*
8	0.259	0.018	−0.006	0.035	−0.033	0.236	0	−0.036	0.001	*0.091*
9	0.227	0	0	0	0	0.227	0	0	0	0
10	0.189	−0.011	−0.003	0.013	−0.01	0.187	*1.497*	−0.013	0.015	−0.041

Note: Results are presented for bridge with fault crossing between Bent 2 and Bent 3, and bridge on one side of fault.

Table 4. Modal Contribution Factors for Four-Span Unsymmetric Bridge and Strike-Slip Fault

	Bridge without shear keys					Bridge with shear keys				
		Across Fault		*SU*			Across fault		One side	
Mode	Period (s)	Bent 2 drift	Abut 1 disp.	Bent 2 drift	Abut 1 disp.	Period (s)	Bent 2 drift	Abut 1 disp.	Bent 2 drift	Abut 1 disp.
1	0.839	*−4.344*	*−0.799*	*0.791*	*0.691*	0.660	*−6.871*	*−0.673*	*0.840*	*0.797*
2	0.556	*5.534*	*1.809*	*0.067*	*0.104*	0.347	*7.387*	*1.299*	0.020	0.033
3	0.327	0	0	0	0	0.327	0	0	0	0
4	0.307	*−0.332*	*−0.114*	*0.076*	*0.124*	0.286	0	0	0	0
5	0.286	0	0	0	0	0.278	*−0.466*	*0.102*	0.017	−0.036
6	0.209	0	0	0	0	0.209	0	0	0	0
7	0.204	*0.129*	*0.064*	*0.050*	*0.118*	0.191	*0.447*	*0.062*	*0.102*	*0.138*
8	0.194	0.019	0.005	0.019	−0.022	0.179	0.074	−0.024	0.022	*0.069*
9	0.161	0.031	0.034	−0.003	−0.015	0.155	*0.578*	*0.229*	0	−0.002
10	0.115	0	0	0	0	0.115	0.002	0.001	0	0

Note: Results are presented for bridge with fault crossing between Bent 2 and Bent 3, and bridge on one side of fault.

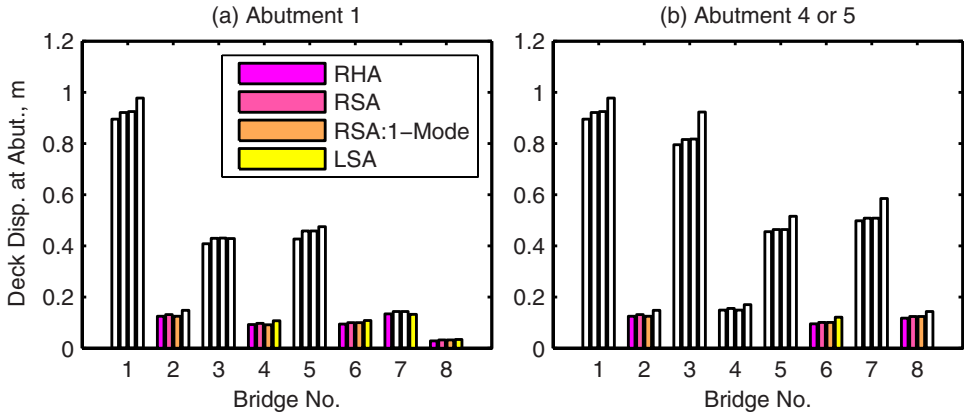

Fig. 12. Comparison of transverse deck displacement at abutments determined by three proposed procedures—RSA, RSA:1-Mode, and linear static analysis (LSA)—with those from the exact RHA procedure. Results are for fault-parallel ground motions associated with a vertical strike-slip fault.

with modal contribution factors >0.05 are also identified with italic font. These results permit several important observations on the type and number of modes that need to be considered for the dynamic analysis.

First, the types of vibration modes excited in bridges crossing fault-rupture zones are entirely different from the modes excited in bridges on one side of the fault: for a three-span symmetric bridge, predominantly torsional modes are excited in the first cases, whereas only transverse modes are excited in the second case. The modal contribution factors are non zero only for the torsional modes of the bridge crossing a fault—second and sixth modes for the bridge without shear keys and third and fifth mode for the bridge with elastic shear keys [see Table 1 and Figs. 8(a and b)]; and are nonzero only for transverse modes in the case of the bridge on one side of the fault—first and fifth modes for the bridge without shear keys, and first and sixth modes for bridge with elastic shear keys [see Table 1 and Figs. 8(a and b)]. For the other three bridges, the modal contribution is largest for predominantly torsional modes in the case of bridges crossing faults and for predominantly transverse modes in the case of bridges on one side of the fault (Tables 2–4), indicating that the contribution of such modes would be largest.

Second, many more modes may be required to accurately estimate the seismic demands in bridges with elastic shear keys compared to those without shear keys and in unsymmetric bridges compared to symmetric bridges. For example, the modal contribution factor for the three-span symmetric bridge crossing a fault is significant only for one mode in the case of a bridge without shear keys but for two modes for bridge with elastic shear keys (Table 1). For the three-span unsymmetric bridge without shear keys crossing a fault, it is significant for four modes (Table 2) compared to only one mode for its symmetric counterpart (Table 1). Similar trends are observed for the four-span bridge (Tables 3 and 4).

Third, the number and types of modes to be included in dynamic analysis may depend on the seismic demand being evaluated. For example, the first and second modes may be sufficient to estimate the drift in Bent 2 of the four-span symmetric bridge without shear keys crossing a fault, whereas three modes—first, second, and fifth—may be necessary to estimate the deck displacement at Abutment 1 (Table 4).

Finally, the modal contribution factors may be larger than 1.0 for some modes and negative for other modes (Tables 2–4); opposing algebraic signs indicate cancellation of modal responses.

Accuracy of Proposed Procedures

The procedures presented to estimate the peak response are based on two approximations: (1) superposing the peak values of quasi-static and dynamic responses [Eq. (17)]; and (2) estimating the peak dynamic response by the RSA or the linear static analysis procedure. In this section, the combined errors due to both approximations are investigated by comparing the peak values of

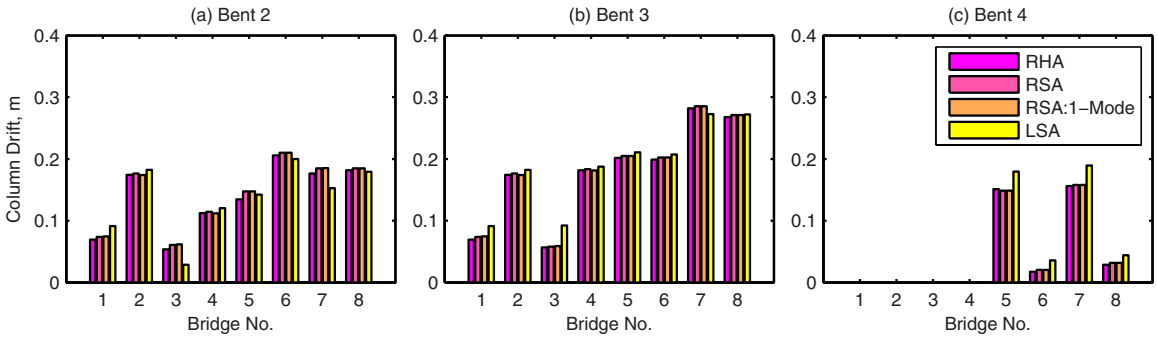

Fig. 13. Comparison of transverse column drifts determined by the three proposed procedures—RSA, RSA:1-Mode, and linear static analysis (LSA)—with those from the exact RHA procedure. Results are for fault-parallel ground motions associated with a vertical strike-slip fault.

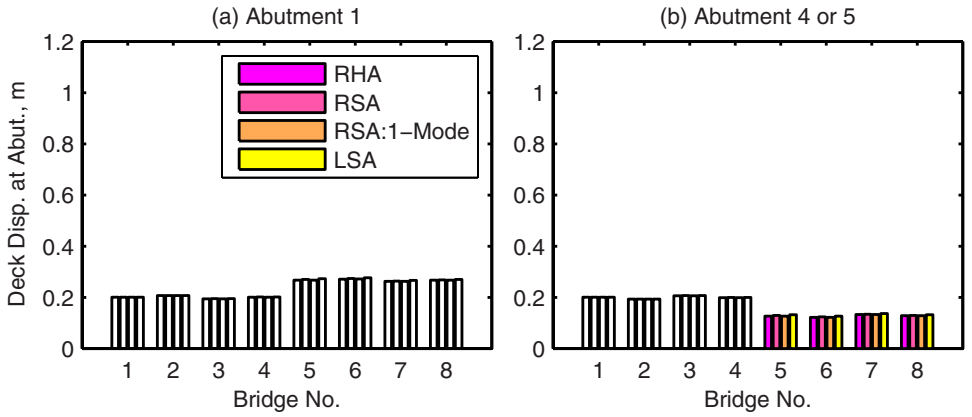

Fig. 14. Comparison of longitudinal deck displacement at abutments determined by the three proposed procedures—RSA, RSA:1-Mode, and linear static analysis (LSA)—with those from the exact RHA procedure. Results are for fault-normal ground motions associated with a fault with dip of 40° and rake of 110°.

the responses determined by approximate procedures and by the RHA [Eq. (15)], the exact procedure. For this purpose, presented are the transverse responses of bridges due to fault-parallel motions resulting from a rupture on a vertical strike-slip fault (Figs. 12 and 13), and the longitudinal responses due to fault-normal motions resulting from a rupture on a fault with a dip of 40° and rake of 110° (Figs. 14 and 15). Note that for the selected bridges and orientation of the fault, fault-parallel ground motions cause response only in the transverse direction of the bridge and fault-normal motions lead to response only in the longitudinal direction of the bridge. Also included are results from the RSA procedure considering contribution of only the dominant mode, the mode with the largest modal contribution factor; these results are denoted as RSA:1-Mode.

The presented results show that both versions of the RSA lead to estimates of seismic demands that are very close to those from the exact RHA procedure, indicating that the most-dominant mode contributes essentially all of the dynamic response of the selected systems.

The presented results also show that the linear static analysis procedure that avoids dynamic analysis also provides a reasonably good estimate of the seismic demand, which is slightly conservative in most cases. Such an overestimation is expected because the simplified procedure is based on an upper bound estimate of the pseudoacceleration=$2.5\ddot{u}_{go}$. However, it underestimates the seismic demand slightly in a few cases, e.g., Bent 2 drift for Bridges 3 and 7 [Fig. 13(a)] because these bridges have two nearly most-dominant modes and contribution of these two modes to some seismic demands tend to cancel out.

Comments on Procedure Based on Fault-Rupture Load Cases

Gloyd et al. (2002) proposed a simple design approach for ordinary bridges crossing fault-rupture zones by consider the following two load cases, in addition to the standard CALTRANS Load Cases I–VII:

$$\text{Group VII}_{\text{FR-1}} = 1.0[1.0D + \beta_E E + 1.0B + 1.0\text{SF} + 1.0\text{PS} + 1.0\text{EQ} + 1.0\text{FR}_P] \tag{18a}$$

$$\text{Group VII}_{\text{FR-2}} = 1.0[1.0D + \beta_E E + 1.0B + 1.0\text{SF} + 1.0\text{PS} + 1.0\text{FR}_D] \tag{18b}$$

in which D, E, B, SF, PS, EQ, FR_P, and FR_D are demands due to dead load, earth pressure, buoyancy load, stream-flow load, prestress load, earthquake load, probabilistic surface displacement (or fault-offset), and deterministic fault-offset, respectively, and β_E=load multiplier for earth pressure. (1) The $\text{VII}_{\text{FR-1}}$ load case involves superposition of demands FR_P from static analysis of the bridge due to the fault-offset, estimated from probabilistic analy-

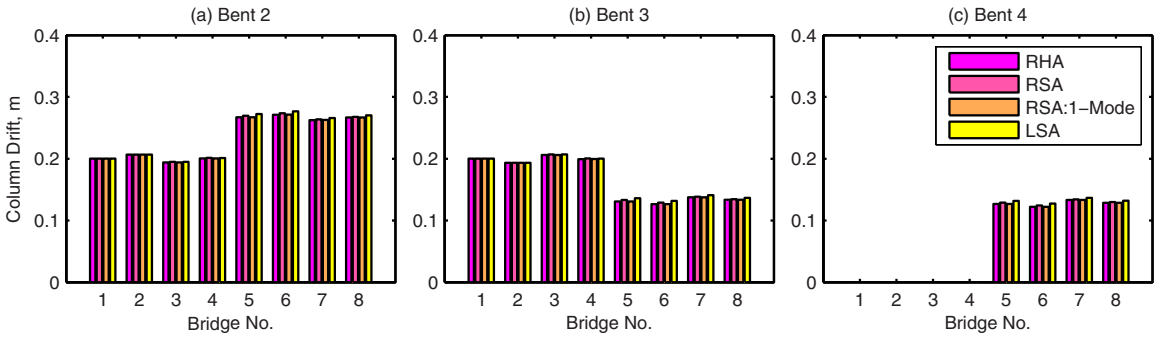

Fig. 15. Comparison of longitudinal column drifts determined by the three proposed procedures—RSA, RSA:1-Mode, and linear static analysis (LSA)—with those from the exact RHA procedure. Results are for fault-normal ground motions associated with a fault with dip of 40° and rake of 110°.

sis, in the fault-parallel direction and EQ from dynamic analysis of the bridge to motions in the fault-normal direction. (2) Load case $VII_{FR\text{-}2}$ involves only demand FR_D from static analysis of the bridge to the fault-offset, estimated from deterministic analysis, in the fault-parallel direction.

In contrast, the structural-dynamics-based development presented in this paper demonstrates that analysis of bridges crossing fault-rupture zones due to an individual component of ground motion (fault-parallel or fault-normal) requires superposition of demands from a static analysis for fault-offset and a dynamic analysis for spatially varying ground motion.

Although the procedure proposed by Glyod et al. (2002) considers the static response due to fault offset, it either ignores the dynamic response or considers the dynamic response incorrectly. For example, the $VII_{FR\text{-}1}$ load case combines the static response due to fault offset in the fault-parallel direction with the dynamic response due to excitation in the fault-normal direction. Obviously, the dynamic part of the response due to ground shaking in the fault-parallel direction is ignored in this load case. The $VII_{FR\text{-}2}$ load case ignores the dynamic response due to both fault-parallel and fault-normal ground motions.

Conclusions and Recommendations

This investigation has led to development of two procedures—RSA procedure and linear static analysis procedure—for estimating peak responses of linearly elastic ordinary bridges crossing fault-rupture zones. Although much simpler than response history analysis, these procedures provide estimates of peak seismic responses that are sufficiently "accurate" for most practical application.

The presented procedures idealize spatially varying excitation as a proportional multiple-support excitation in which motions at various supports of the bridge are assumed to be proportional to the motion at a reference location. It has been demonstrated that this idealization is valid for spatially varying ground motions in close proximity to faults with various dip and rake angles, and provides accurate estimates of peak seismic responses.

In the presented procedures, the peak value of seismic response of the bridge is computed by superposition of peak values of quasi-static and dynamic parts of the response. The peak quasi-static response is computed by static analysis of the bridge with peak values of all support displacements applied simultaneously. Two procedures are presented for estimating the peak dynamic response. In the RSA procedure it is estimated directly from the response spectrum including all significant modes in the dynamic analysis. The linear static analysis procedure avoids computing the vibration periods of the bridge as well as estimating the rise time of the fault offset, and estimates the peak dynamic response by a much simpler static analysis of the bridge to appropriately selected forces. These procedures utilize the effective influence vector that differs from that for the spatially uniform excitation. Further, the RSA procedure uses the response spectrum for ground motions expected in close proximity to the causative fault.

The natural vibration modes that are excited in bridges subjected to motions resulting from rupture on a fault passing under the bridge differ entirely from those excited in bridges on one side of the fault. Therefore, it is important to correctly identify the modes that need to be considered in the RSA procedure. For this purpose, the modal contribution factor concept is demonstrated to be useful.

It is shown that both the RSA procedure and the linear static analysis procedure provide estimates of peak total response that are very close to the peak response determined by exact response history analysis. Further, it is shown that only one mode the most dominant mode—is usually sufficient in the RSA procedure.

It is also demonstrated that procedures currently being used by bridge engineers are inappropriate for estimating seismic demands in bridges crossing fault-rupture zones: these procedures either ignore the dynamic part of the response or compute it incorrectly.

It is recognized that bridges subjected to motions resulting from rupture of a fault passing under the bridge are unlikely to remain within the linear elastic range. Therefore, the research reported in this paper must be viewed as the basis for development of a procedure to estimate seismic demands in bridges responding beyond the linearly elastic range, a subject addressed in the companion paper (Goel and Chopra 2009).

Acknowledgments

The research reported in this paper is supported by California Department of Transportation, Sacramento under Contract No. 59A0435 with Mahmoud Khojasteh as the project manager. This support is gratefully acknowledged. Also acknowledged is the assistance of Douglas Dreger and Mr. Gabriel Hurtado of University of California, Berkeley who generated the ground motions used in this investigation.

References

CALTRANS. (2006). *Seismic design criteria*, Version 1.4.

Chopra, A. (2007). *Dynamics of structures: Theory and applications to earthquake engineering*, 3rd Ed., Prentice-Hall, Englewood, N.J.

Der Kiureghian, A., and Neuenhofer, A. (1992). "Response spectrum method for multiple support seismic excitation." *Earthquake Eng. Struct. Dyn.*, 21(8), 713–740.

Dreger, D., Hurtado, G., Chopra, A., and Larsen, S. (2007). "Near-fault seismic ground motions." *Rep. No. UCB/EERC-2007/03*, Earthquake Engineering Research Center, Univ. of California, Berkeley, Calif.

Earthquake Engineering Research Institute (EERI). (2000). "Chapter 18: Impact on highway structures in Kocaeli, Turkey, earthquake of August 17, 1999 reconnaissance report." *Earthquake Spectra*, Supplement A to Volume 16.

Earthquake Engineering Research Institute (EERI). (2001). "Chapter 8: Highway bridges in Chi-Chi, Taiwan, earthquake of September 21, 1999 reconnaissance report." *Earthquake Spectra*, Supplement A to Volume 17.

Ghasemi, H., Cooper, J. D., Imbsen, R., Piskin, H., Inal, F., and Tiras, A. (2000). "The November 1999 Duzce Earthquake: Post-Earthquake Investigation of the Structures in the TEM." *Publication No. FHwA-RD-00-146*, U.S. Dept. of Transportation, Federal Highway Administration, Washington, D.C.

Gloyd, S., Fares, R., Sánchez, A., and Trinh, C. (2002). "Designing ordinary bridges for ground fault rupture." *Proc., 3rd National Seismic Conf. and Workshop on Bridges and Highways*, *Rep. No. MCEER-02–SP04*, Multidisciplinary Center for Earthquake Engineering Research, Univ. at Buffalo, Buffalo, N.Y.

Goel, R. K., and Chopra, A. K. (2008a). "Analysis of ordinary bridges crossing fault-rupture zones." *Rep. No. UCB/EERC-2008/01*, Earthquake Engineering Research Center, Univ. of California, Berkeley, Calif.

Goel, R. K., and Chopra, A. K. (2008b). "Role of shear keys in seismic behavior of bridges crossing fault-rupture zones." *J. Bridge Eng.*,

13(4), 398–408.

Goel, R. K., and Chopra, A. K. (2009). "Nonlinear analysis of ordinary bridges crossing fault-rupture zones." *J. Bridge Eng.*, 14(3), 216–224.

McKenna, F., and Fenves, G. (2001). *The OpenSees command language manual: Version 1.2*, Pacific Earthquake Engineering Center, Univ. of California, Berkeley, Calif., ⟨http://opensees.berkeley.edu⟩.

Somerville, P. G., et al. (1999). "Characterizing crustal earthquake slip models for the prediction of strong ground motion." *Seismol. Res. Lett.*, 70(1), 59–80.

Yen, W.-H. (2002). "Lessons learned about bridges from earthquake in Taiwan." *Public roads*, U.S. Dept. of Transportation, Federal Highway Administration, 65(4).